Journal of Materials Chemistry A

Accepted Manuscript

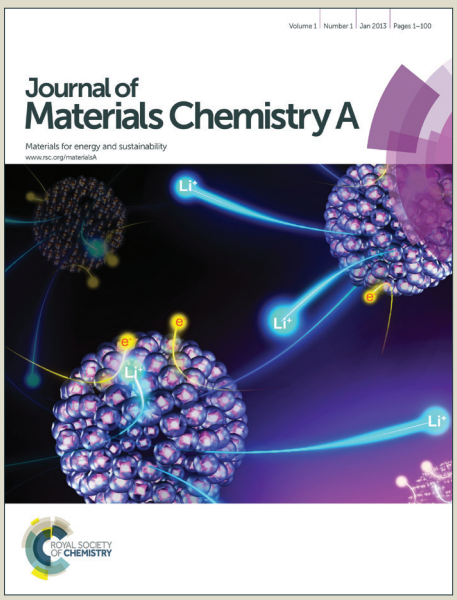

ROYAL SOCIETY OF CHEMISTRY

www.rsc.org/materialsA

Journal of Materials Chemistry A RSCPublishing

ARTICLE

Water Sensitivity of Layered P2/P3-$Na_xNi_{0.22}Co_{0.11}Mn_{0.66}O_2$ Cathode Material

Cite this: DOI: 10.1039/xoxxoooooox

Daniel Buchholz[1,2], Luciana Gomes Chagas[1,2], Christoph Vaalma[1,2], Liming Wu[1,2], Stefano Passerini[1,2*]

Received ooth January 201X,
Accepted ooth January 201X

DOI: 10.1039/xoxxoooooox

www.rsc.org/

Sodium-based layered oxides undergo several structural changes upon the (de-)sodiation process and reveal a strong tendency towards water intercalation at lower sodium contents. However, valuable information about their handling during the investigation are still rare. Herein, we report an investigation of the water sensitivity of layered $Na_xNi_{0.22}Co_{0.11}Mn_{0.66}O_2$ with mixed P2/P3 structure via X-ray diffraction. At lower sodium contents, i.e. below $x \approx 0.33$ or above 3.6 V vs. Na/Na^+, a strong tendency for the uptake of water is observed, supported by the appearance of new diffractions peaks confirming a dramatically increased interlayer distance. However, at high sodium content ($x > 0.33$) the material can be processed in open air without major changes.

1. Introduction

The interest in sodium-ion batteries is rapidly increasing since the technology appears to offer certain advantages compared to the lithium-ion battery one.[1-4] Sodium is not only cheaper than lithium but also widely distributed, thus enabling worldwide mining for sodium raw materials. Additionally, aluminium is usable as anode current collector, underlining the low cost aspect of the sodium-ion battery.[5]

Suitable electrochemical performance has been demonstrated for various sodium based cathode and anode materials, often superior to that of presently known secondary battery materials.[6-8] Layered cathode materials have been intensively investigated due to their known good electrochemical performance in the sodium batteries.[9-16] Generally, layered sodium-based cathode materials can be classified for the sodium cations coordination geometry (O=octahedral, P=prismatic, T=tetrahedral) followed by a digit indicating the number of transition metal layers per unit cell. One of the most interesting differences between lithium and sodium hosts consists in the larger ionic radius of the sodium cation, which enables trigonal prismatic as well as octahedral coordination. This is the origin of the several differences observed upon the whole (de-)intercalation process of sodium layered hosts compared to layered lithium-ion cathode materials. Changing the coordination of the sodium cation from trigonal prismatic to octahedral, e.g. from a P2 (prismatic coordination of Na^+ ions, two MO_2-layers per unit cell) to an O3 host structure, leads to tremendous differences concerning the electrochemical behaviour in terms of reversible specific capacity and cycling performance. In more detail, it has been demonstrated by Komaba et al. that the behaviour of P2- and O3- $Na_x[Fe_{0.5}Mn_{0.5}]O_2$ is very different, whereby the P2-type material reveals a much better electrochemical performance.[14] In addition, Tarascon et al. have observed a high irreversibility when O3-$NaNi_{1/3}Mn_{1/3}Co_{1/3}O_2$ is cycled to potentials above 4.0 V vs. Na/Na^+. Good electrochemical performance was obtained with this material only at lower potentials.[11]

Different coordination of the sodium cation as well as layer stacking in the cathode materials (P2-, P3-, or O3- type structures) can be obtained chemically varying the annealing temperature, type and ratio of the transition metals, and sodium content.[17-20] The latter parameter can be changed also by electrochemical means. The large sodium cation provides layered oxides with the ability to undergo phase transitions upon the (de-)sodiation process, as a function of the electrode potential and sodium content inside the material.[21-24] Early in-situ X-ray diffraction measurements of P2-$Na_{2/3}[Ni_{1/3}Mn_{2/3}]O_2$ by Lu and Dahn revealed that pure P-based materials undergo a phase transition at low sodium contents (i.e., high potentials) to the corresponding O-based material, via the gliding of the transition metal layers induced by the increased oxygen repulsion of adjacent layers. This mostly reversible phase transition is accompanied by a dramatic change of the c-axis parameter, being a good indication for this phase transition.[23] Recently, structural investigations for P2-$Na_xNi_{0.5}Fe_{0.5}O_2$ have shown that also the phase transition from P2 into a complex stacked, fault OP4 structure might have to be considered at lower sodium contents (i.e., high potentials vs. Na/Na^+).[14] O3-type materials (e.g. $NaNi_{1/3}Mn_{1/3}Co_{1/3}O_2$ or $Na_{1-x}[Ni_{0.5}Mn_{0.5}]O_2$) also show several phases and, thus, phase transitions in dependence of the sodium content, which were

identified via X-ray diffraction.[11,22] In addition to these electrochemically induced phase transitions, layered sodium-based oxides show a strong tendency towards water intercalation and the formation of hydrated phases at lower sodium contents.[11, 22, 25-32] So far, a detailed study on the occurrence of hydrated phase, which formation requires special care for handling of sodium-based layered oxides in air, is missing. In the past we have developed the synthesis of P2-$Na_{0.45}Ni_{0.22}Co_{0.11}Mn_{0.66}O_2$ exhibiting an excellent electrochemical performance.[9] Very recently, we have synthesized $Na_xNi_{0.22}Co_{0.11}Mn_{0.66}O_2$ with mixed P2/P3 structure and characterized its electrochemical behaviour in combination with an ionic liquid-based electrolyte.[13] Both synthesis procedures involved a water rinsing step to enhance the materials purity and improve the electrochemical performance. No evidence of water intercalation was observed in these materials.

Herein, we present an ex-situ X-ray diffraction study on $Na_xNi_{0.22}Co_{0.11}Mn_{0.66}O_2$ cathode material with mixed P2/P3 structure in order to shed some light on its water sensitivity. Main target of this work is to provide information about the crucial sodium content at which the hydrated phase is formed and when care must be taken to handle, investigate or synthesize these materials in air. This study provides very valuable, basic information of importance for the growing research field of sodium-ion batteries.

2. Experimental Section

Synthesis of P2/P3- $Na_xNi_{0.22}Co_{0.11}Mn_{0.66}O_2$

The material was synthesized via a solid-state reaction method from sodium hydroxide (NaOH, Aldrich >98%) and a manganese-nickel-cobalt hydroxide precursor. This latter compound was prepared by co-precipitating the aqueous solution of the three metal acetate salts, Mn, Ni, and Co (Aldrich > 98%) in the weight ratio 66:22:11, with sodium hydroxide (50% excess). After extensive rinsing with distilled water, the precipitate was dried under vacuum at 120 °C overnight. The dried material was then dispersed in an aqueous solution of sodium hydroxide (0.76 eq. of NaOH per mole of $Ni_{0.22}Co_{0.11}Mn_{0.66}(OH)_2$). Water was slowly removed in a rotary evaporator. After drying and grinding, the mixture was annealed in air at 500 °C for 5 h, and then at 750°C for 6 h, using an open-air muffle oven. Afterwards the material was ground, screened over a 45 µm sieve and, finally, stored under inert atmosphere. For the water treatment about 1 g of the as-prepared material was stirred in 20 mL of distilled water at 25 °C for five minutes. The suspension was then filtered and washed with 80 mL of distilled water, dried at 120 °C in air for 24 hours and finally, stored under inert atmosphere.

Characterization

The ex-situ X-ray diffraction study was performed using the Cu K_α radiation on the D8 Advance (Bruker) in Bragg-Brentano geometry in the 2θ range from 10° to 90°. Lattice parameters were determined by Rietveld refinement with TOPAS software (Bruker).

Electrodes were prepared by casting slurries, which solid content was: 85 wt.% active material, 10 wt.% Super C65 (TIMCAL), and 5 wt.% PVdF (6020 Solef®, Arkema Group), onto Al foil. The active material mass loading of the electrodes was about 2 mg cm^{-2}. Sodium metal was used as counter and reference electrodes. Sodium chunks (99.8%, Acros Organics) were rolled and pressed to form a foil, which was finally punched on the current collector. The cathode electrodes were assembled into Swagelok cells with the 1 M solution of $NaPF_6$ (99%, Sigma-Aldrich) in propylene carbonate (UBE, Japan), as the electrolyte. Cells were cycled galvanostatically at a current rate of 0.1C (nominal capacity = 122 mA h g^{-1}, 0.1C = 12.2 mA g^{-1}) between 4.6 V and 1.5 V at 20°C using Maccor series 4000 battery tester (USA). All potential reported in this work refer to the Na/Na^+ couple.

For the in-situ X-ray diffraction study a modified coin cell was assembled with sodium as counter electrode. The mixture of active material, conductive agent and binder was dried and then coated on Kapton foil, previously sputtered with aluminium, simultaneously serving as current collector and transparent window for the X-ray beam. The coated Kapton foil was subsequently dried at 80 °C for 10 minutes and 40 °C under vacuum over night. The cell was then galvanostatically charged (0.05C rate, 6 mA g^{-1}) up to 4.6 V while collecting XRD spectra within the 2θ range from 10° to 60° with a step size of 0.03°and a time per step of 0.5sec (complete scan every 30 minutes).

For the ex-situ X-ray diffraction study, the sodium half-cells were cycled for two cycles at 0.1C (12.2 mA g^{-1}) between 4.6-1.5 V (vs Na/Na^+). Afterwards, the cells were charged (desodiated) up to a chosen potential. Finally, the cells were transferred into an argon-filled glovebox and disassembled. The positive electrodes were removed, rinsed with dimethylcarbonate (DMC, UBE, Japan) and then stored in the argon-filled glovebox. Finally, the rinsed electrodes were exposed to air and X-ray diffractograms were recorded. Schematic illustrations of the structures have been created using DIAMOND program.

3. Results and Discussion

X-ray diffraction patterns of pristine $Na_{0.45}Ni_{0.22}Co_{0.11}Mn_{0.66}O_2$ as well as that of a composite electrode are shown in Fig. 1. Further details of the structural, morphological and electrochemical characterization of P2- and mixed P2/P3-$Na_{0.45}Ni_{0.22}Co_{0.11}Mn_{0.66}O_2$ can be found in our previous works.[9,10,13]

The XRD diffractogram reveals that $Na_xNi_{0.22}Co_{0.11}Mn_{0.66}O_2$ synthesized at 750°C consists of a mixture of P2- and P3- structures (Fig. 1), whereby the $(00l)$ reflections for the P2 and P3 layered compounds are superimposed, which finally leads to one set of broadened $(00l)$ reflections.[13] Therefore, both space groups were used for the Rietveld refinement.[19,33] The calculated lattice parameters

were a= 2.86095(15)Å and c=16.8234(21)Å for the P3-component (space group: R3m) and a=2.859376(98) Å and c=11.19069(75)Å for the P2- component (space group: $P6_3/mmc$). More detailed information about the Rietveld refinement can be found in the supporting information.

The diffractogram of the electrode obtained from the pristine P2/P3 $Na_{0.45}Ni_{0.22}Co_{0.11}Mn_{0.66}O_2$ material is shown in (Fig. 1b). Due to strong preferred orientation of the particles in the pressed electrode the $(00l)$ reflections are clearly visible while

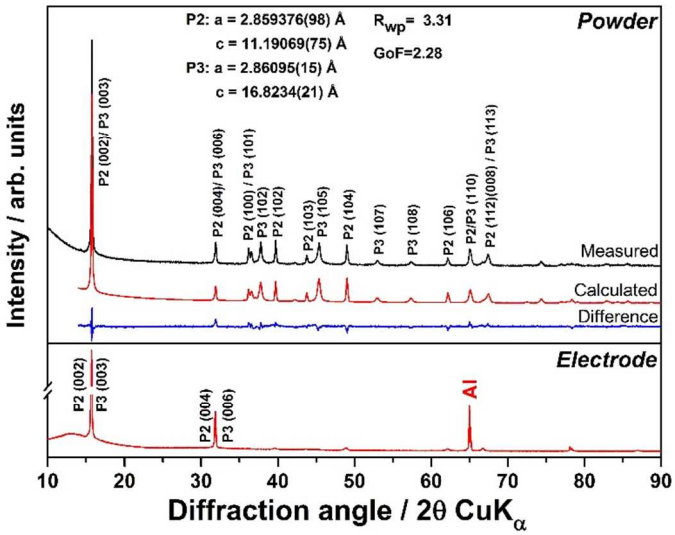

Fig. 1 X-ray diffraction pattern and Rietveld refinement of the pristine powder of P2/P3-$Na_{0.45}Ni_{0.22}Co_{0.11}Mn_{0.66}O_2$ synthesized at 750°C (upper plot) and X-ray diffraction pattern of the pristine electrode of P2/P3-$Na_{0.45}Ni_{0.22}Co_{0.11}Mn_{0.66}O_2$.(lower plot)

all other $(10l)$ diffraction peaks are strongly reduced in intensity. Therefore, the $(00l)$ reflexes, occurring in the 2θ range from 10°-38° were used for the evaluation of the structural changes taking place in the material upon desodiation of the electrodes. The diffraction peak of the aluminium current collector, at 2θ = 65.1°, was used as an internal reference for the normalization of the electrode diffraction patterns. Further diffraction peaks of the aluminium foil are located at 38.46°, 44.73°, 53.20° and 58.20°. A schematic illustration of the P2 and the P3 structures can be found in Fig. 2.

In these structures the transition metals are coordinated octahedrally and intermixed inside the transition metal layers. Past studies have shown that superlattice ordering of the cations might be considered in dependence of the transition metal ratio.[20] In addition, also oxygen vacancies and cation mixing might occur as well.[36] In analogy to layered lithium-based transition metal oxides the average oxidation state of nickel, cobalt and manganese is considered to be 2+, 3+ and 4+, respectively.[17,35] In the P2-type material (Fig. 2a) two sodium sites are present, in which sodium ions are coordinated in a trigonal prismatic manner by six oxygen anions. One sodium cation site (dark greyish in Fig. 2a) is located between two transition metal cations in adjacent layers, leading to an additional electrostatic repulsion. The second sodium cation (light greyish) is located between two oxygens in adjacent layers. This site is energetically favoured and mainly, if not exclusively, occupied at low sodium contents. On the other hand, the P3-type structure (Fig. 2b) offers only a sodium cation site because the transition metal layers are stacked in a different way. Of further importance for P2- and P3-type structures is the electrostatic repulsion of the sodium cations, which is leading to several different arrangements within the sodium layer, also occurring within very minor changes of sodium content. [25, 26, 33-35]

In-situ and ex-situ diffraction patterns were acquired using a sealed cell or sealed electrode, respectively, in order to verify the desodiation process (Fig. 3a-c). The voltage profile recorded

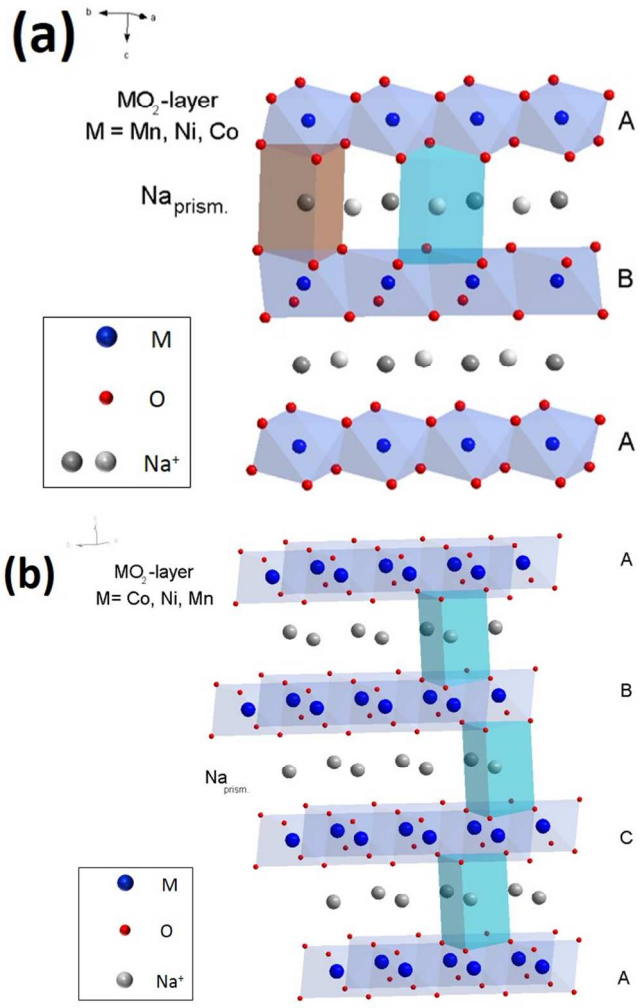

Fig. 2 Schematic illustration of the a) P2-type or b) P3-type structure of $Na_{0.45}Ni_{0.22}Co_{0.11}Mn_{0.66}O_2$.

during the first desodiation step, illustrated in Fig. 3a, is that typical of P2/P3 $Na_{0.45}Ni_{0.22}Co_{0.11}Mn_{0.66}O_2$.[13]

The X-ray diffractogram obtained from the in-situ cell reveals three very broad reflections, marked with asterisks,

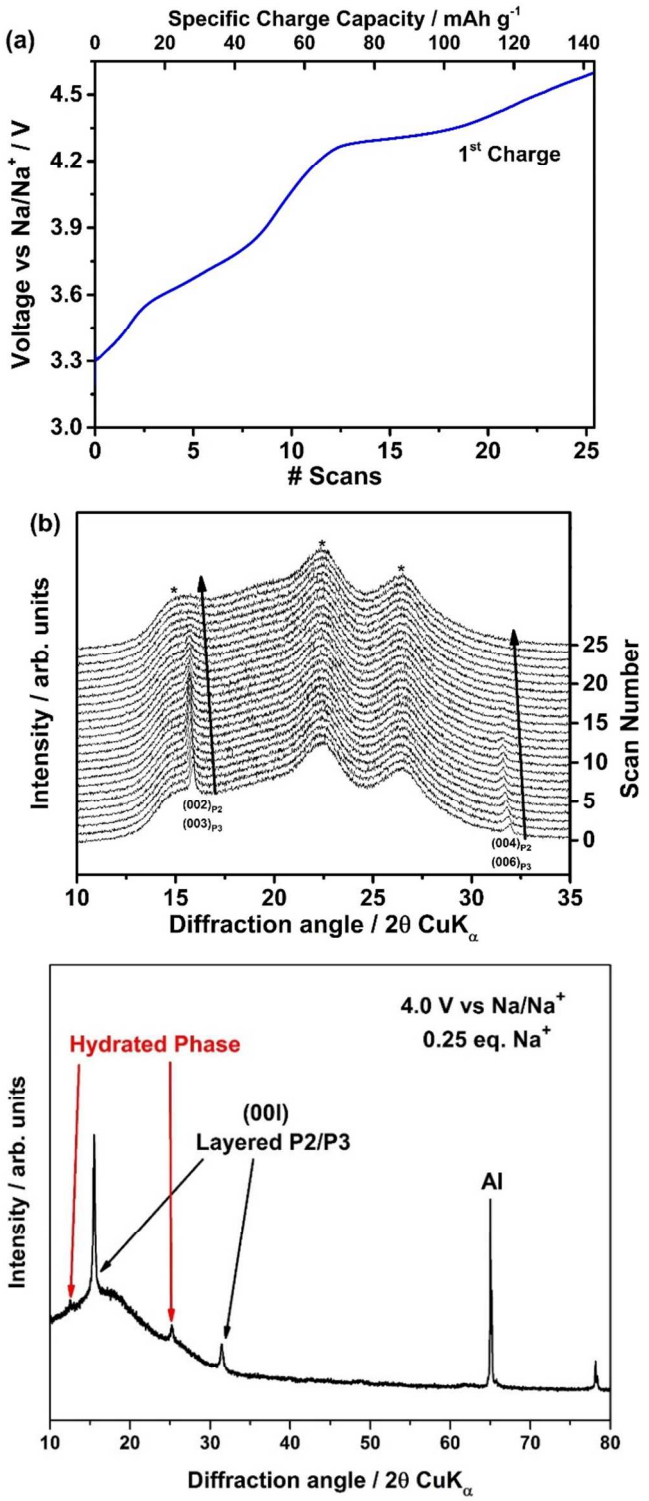

Fig. 3 a,b) In-situ X-ray diffraction patterns obtained in the range of 10-35° 2θ and corresponding voltage profile for the initial charge process of P2/P3-$Na_xNi_{0.22}Co_{0.11}Mn_{0.66}O_2$. c) Ex-situ X-ray diffraction pattern of sealed P2/P3-$Na_xNi_{0.22}Co_{0.11}Mn_{0.66}O_2$ electrodes in the range of 10-80° 2θ. In-situ X-ray diffractograms were obtained at different states of charge within the first cycle, while the ex-situ diffractogram refers to a partially charged electrode (x ≈ 0.25; 4.0 V vs. Na/Na^+).

originating from the Kapton tape (Figure 3b). Besides those, the overlapping $(002)_{P2}/(003)_{P3}$ and $(004)_{P2}/(006)_{P3}$ reflections of the two P-type structures are observed. Upon desodiation a regular shift towards lower angles is observed for both reflection sets. This general shift is in accordance with previous in-situ studies on similar layered sodium oxides,[21,23,24] which are correlated to an increasing interlayer distance, i.e., an increasing c-axis parameter, caused by the increasing repulsion of the oxygen anions in the trigonal prismatic coordination. Upon further desodiation, a continuous broadening of the $(00l)$ reflections can be observed. At high potentials of about 4.3 V vs. Na/Na^+ (scan no. 21-25), the $(00l)$ reflections finally disappear indicating the phase transition from the P to the O phases. Due to the high intensity of the Kapton tape reflections and the different possibilities in which adjacent layers in prismatic configuration can glide, the corresponding reflections of the O-phase are not visible. Comparing these results with those (Fig. 3c) obtained ex-situ for a sealed electrode of P2/P3-$Na_xNi_{0.22}Co_{0.11}Mn_{0.66}O_2$ at x ≈ 0.25 (4.0 V vs. Na/Na^+) reveals the strong tendency for water uptake of P-type layered cathode material. In fact, beside the $(00l)$ reflections, two additional features at 2θ = 12.56° and 2θ = 25.30° can be seen, which are to be assigned to the intercalation of water (further marked as $(hkl)'$ reflections). Similar interlayer distances have been reported by Lu and Dahn for similar layered P2-$Na_{2/3}[Co_xNi_{1/3-x}Mn_{2/3}]O_2$ upon exposure to water or humid air.[30] Rietveld refinements indicated that the water molecules are located in free sites within the sodium layers, which, in this way, simultaneously stabilize the high repulsion of adjacent oxygen layers via the formation of hydrogen bridge bonds. Summarizing, a combination of increased electrostatic repulsion of neighbouring oxygen layers and empty sodium sites are the driving force enabling the observed water intercalation.

Fig. 4 depicts the voltage profile of P2/P3-$Na_xNi_{0.22}Co_{0.11}Mn_{0.66}O_2$ during charge, i.e., desodiation, as a function of the sodium content.

The voltage profile recorded at 0.1C, exhibits several features, with those occurring between 3.8 and 1.5 V related to cation vacancy ordering occurring within the sodium layers upon desodiation. The driving force for this vacancy ordering is the electrostatic repulsion of the sodium cations or, in case of the P2-type material, the occupation of the favoured sites.[23,25-29] The features at potentials lower than 2.5 V are related to the Mn^{3+}/Mn^{4+} redox process.[10] The plateau at high voltage (4.2 V *vs.* Na) is, on the other hand, correlated with the phase transition from P-type to O-type, occurring at low sodium contents in the material with the gliding of the transition metal layers.

The arrows in Figure 4 indicate the voltages at which the electrodes were desodiated for the ex-situ investigation. Ex-situ XRD patterns were taken for electrodes with sodium content (x) of 0.79, 0.71, 0.63, 0.50, 0.41, 0.34, 0.25, 0.07 and 0.00. These values were calculated based on the assumptions that (i) the sodiation/desodiation process is fully reversible and (ii) all

sodium cations are removed form the active material in the fully charged state.[23,24]

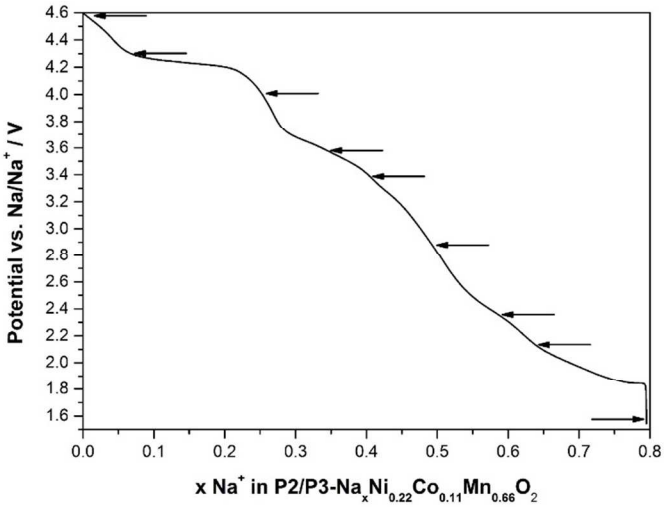

Fig. 4 Potential profile in dependence of the sodium content in P2/P3-$Na_xNi_{0.22}Co_{0.11}Mn_{0.66}O_2$ as detected during the third charge at C/10 (12 mA g^{-1}). Cut-off limits: 4.6 – 1.5 V (*vs.* Na/Na^+). The arrows indicate the potential and composition of the electrode subjected to ex-situ XRD investigation. Reference and counter electrode: Na. Electrolytic solution: 1 M $NaPF_6$ in PC. Scan rate of 0.1 mV s^{-1}. Temperature: 20 °C ± 2 °C

After rinsing, the electrodes were briefly exposed to air and then subjected to XRD examination (Fig. 5). The calculated interlayer distance in dependence of the voltage vs. Na/Na^+ and the sodium content x in P2/P3 $Na_xNi_{0.22}Co_{0.11}Mn_{0.66}O_2$ are given in Table 1.

All diffraction patterns were normalized using the intensity and position of the aluminium diffraction peak (65.1°). At a first glance it is seen that the ex-situ diffraction patterns exhibit large changes of the $(00l)$ reflections upon desodiation. The most remarkable changes occur, however, for x ranging from 0.34 to 0.

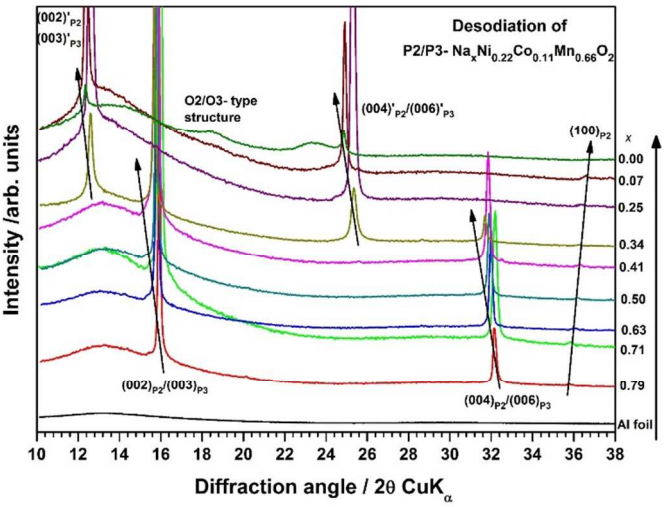

Fig. 5 Ex-situ X-ray diffraction patterns of P2/P3-$Na_xNi_{0.22}Co_{0.11}Mn_{0.66}O_2$ electrodes at different states of charge.

Table 1: Voltage (*vs.* Na/Na^+), sodium content (x in P2/P3-$Na_xNi_{0.22}Co_{0.11}Mn_{0.66}O_2$) and calculated interlayer distance of electrodes at different states of charge investigated via ex-situ X-ray diffraction.

Voltage / V vs. Na/Na^+	x in P2/P3 $Na_xNi_{0.22}Co_{0.11}Mn_{0.66}O_2$	Interlayer Distance / Å
Pristine electrode	0.45	5.6190
1.50	0.79	5.5636
1.95	0.71	5.5497
2.18	0.63	5.6047
2.80	0.50	5.6047
3.37	0.41	5.6187
3.60	0.34	5.6464
3.60	0.34	7.0135
4.00	0.25	7.0356
4.30	0.07	7.1468
4.60	0.00	7.1700
4.60	0.00	4.7983

The $(00l)$ diffraction peaks, giving information about the interlayer distance of the transition metal layers, offer a good opportunity to investigate the structural phenomena upon the desodiation process and the effect of ambient air exposure. At the fully sodiated state (x ≈ 0.79), the $(002)_{P2}/(003)_{P3}$ reflection is located at 15.93°. This feature shifts towards lower angles (to 15.69°) at x ≈ 0.34. The same behaviour is observed for the associated $(004)_{P2}/(006)_{P3}$ and $(008)_{P2}/(0012)_{P3}$ reflections. Additionally, a continuous broadening of the $(002)_{P2}/(003)_{P3}$ feature on going from x ≈ 0.79 to 0.34 takes place, revealing the appearance of stacking faults into the structure as already been reported.[23] More recently, complex stacking was also found for similar layered P2-$Na_x[Fe_{0.5}Mn_{0.5}]O_2$.[14]

At x ≈ 0.34 the onset of two additional reflections $((002)'_{P2}/(003)'_{P3}$ and $(004)'_{P2}/(006)'_{P3})$ is seen, associated to the formation of the hydrated phase. The well-defined peak shape indicates for a very ordered hydrated phase. These reflections can definitely be attributed to the c- direction since they have the high intensity expected from the preferred c-direction orientation of the material in the electrode. The $(002)'_{P2}/(003)'_{P3}$ feature is located at 12.62° and the $(004)'_{P2}/(006)'_{P3}$ at 25.34°. Upon further desodiation of P2/P3-$Na_xNi_{0.22}Co_{0.11}Mn_{0.66}O_2$ (down to x ≈ 0.00) the $(00l)'$ reflections of the hydrated phase shift towards lower angles. Simultaneously, the $(00l)$ reflections completely disappear as expected from the fully desodiated sample. However the $(00l)'$ reflexes are visible, indicating that the electrochemically neutral water intercalation process leads to the, at least partial, replacement of vacancies left by the sodium cations.

Between x ≈ 0.07 and x ≈ 0.00 the P to O phase transition is observed, evidenced by the appearance of a strongly broadened diffraction peak at higher angles (18.49°). This phase transition is necessarily accompanied with massive gliding of the transition metal layers to strongly reduce the repulsion of the oxygen anions in adjacent layers, which is finally leading to a closed-packed configuration. The new reflection at higher angles corresponds to the resulting reduced interlayer distance. Due to the different gliding possibilities of the layers and the continuous introduction of O-type stacking faults a massive peak broadening is observed. Nevertheless, even at 4.6 V still a low amount of water is intercalated in the remaining P-host

structure, as indicated by the persistence of the $(002)'_{P2}/(003)'_{P3}$ diffraction peak at 12.34°. Although, the $(100)_{P2}$ diffraction peak is very weak, its continuous shift towards higher angles (from 35.78° at x ≈ 0.79 to 36.57° at x ≈ 0.00) is seen during the whole desodiation process. This is in accordance with previous investigations, confirming a continuously shrinking of the a-axis parameter, which is not affected by the large changes in the c-direction.[23,24]

The large change occurring in the ex-situ diffraction study of the electrodes exposed to air, however, only appeared at lower sodium contents. The interlayer distance calculated with the Bragg equation well identifies the sodium content below which the spontaneous hydration of P2/P3-$Na_xNi_{0.22}Co_{0.11}Mn_{0.66}O_2$ takes place. The results are summarized in Fig. 6. The amount of water intercalated per formula unit $Na_xNi_{0.22}Co_{0.11}Mn_{0.66}O_2$ is expected to strongly depend on the state of sodiation. However, its determination is an interesting issue for future work.

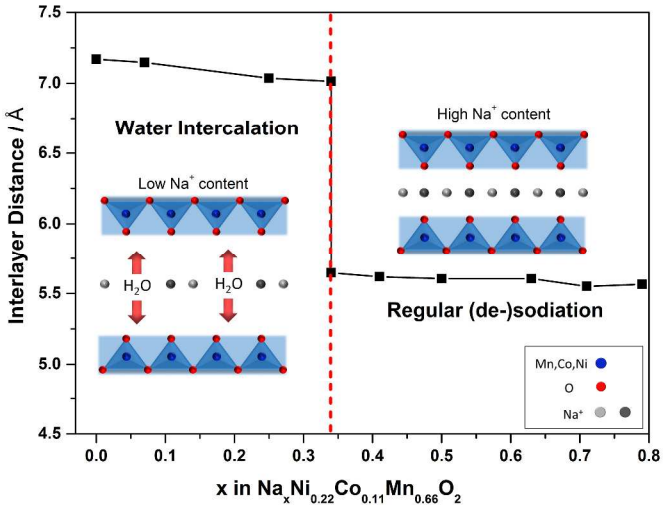

Fig. 6 Calculated Interlayer distance plotted vs. sodium content x in P2/P3-$Na_xNi_{0.22}Co_{0.11}Mn_{0.66}O_2$ electrodes.

4. Conclusions

Layered P2/P3-$Na_{0.45}Ni_{0.22}Co_{0.11}Mn_{0.66}O_2$ material is synthesized via solid state process followed by a water rinsing step. The X-ray diffraction pattern and Rietveld refinement confirmed that a mixed P2-P3 material is obtained at 750°C. The water rinsing does not affect these structures. However, the ex-situ diffraction study on the water sensitivity revealed a strongly increased tendency towards water intercalation for low sodium contents. This is evidenced by the appearance of $(00l)'$ diffraction peaks at lower diffraction angles, corresponding to an abnormally increased interlayer distance. The sodium content of x ≈ 0.33 (sodium-layer half occupied), represents the threshold below which the water insertion takes place. The well defined $(00l)'$ diffraction peaks support the existence of a very ordered hydrated phase.

Acknowledgements

The authors wish to thank the financial support of the European Commission within the FP7-ENERGY-2013-1 Project INFLUENCE (Grant number: 608621). In addition, L. G. C. acknowledges the Conselho Nacional de Desenvolvimento Científico e Tecnológico (CsF-CNPq, Brazil) for the financial support. L. Wu would like to acknowledge the funding from Chinese Scholarship Council (CSC). TIMCAL and ARKEMA is acknowledged for kindly providing SuperC 65 and PVdF Solef® 6020, respectively.

Notes and references

[1]University of Muenster, Institute of Physical Chemistry, Corrensstraße 46, 48149 Muenster, Germany.
[2]Helmholtz Institute Ulm, Albert Einstein Allee 11, 89081 Ulm, German.
*Corresponding author: stefano.passerini@kit.edu

† Footnotes should appear here. These might include comments relevant to but not central to the matter under discussion, limited experimental and spectral data, and crystallographic data.

Electronic Supplementary Information (ESI) available. See DOI: 10.1039/b000000x/

1 V. Palomares, P. Serras, I. Villaluenga, K. B. Hueso, J. Carretero-González, T. Rojo, *Energy Environ. Sci*., 2012, **5**, 5884.
2 J.-M. Tarascon, *Nat. Chem*., 2010, **2**, 510.
3 S.-W. Kim, D.-H. Seo, X. Ma, G. Ceder, K. Kang, *Adv. Energy Mater*., 2012, **2**, 710.
4 H. Kawamoto, W. Tamaki, *Sci. Technol. Trends Q. Rev*., 2011, **39**, 51.
5 H. Baker, H. Okamoto, *ASM Handbook Alloy Phase diagrams*, 1992, **3**, ASM International, USA.
6 H. Pan, Y.-S. Hu, L. Chen, *Energy Environ. Sci*., 2013, **6**, 2338.
7 M.D. Slater, D. Kim, E. Lee, C. S. Johnson, *Adv. Funct. Mater*., 2012, **23**, 947.
8 B.L. Ellis, L.F. Nazar, *Curr. Opin. Solid-State Mater. Sci*., 2012, **16**, 168.
9 D. Buchholz, A. Moretti, R. Kloepsch, S. Nowak, V. Siozios, M. Winter, S. Passerini, *Chem. Mater*. 2013, **25**, 142.
10 D. Buchholz, L.G. Chagas, M. Winter, S. Passerini, *Electrochim. Acta*, 2013, **110**, 208.
11 M. Sathiya, K. Hemalatha, K. Ramesha, J.-M. Tarascon, A.S. Prakash, *Chem. Mater.,* 2012, ***24,*** 1846.
12 D. Kim, E. Lee, M. Slater, W. Lu, S. Rood, C.S. Johnson, *Electrochem. Commun*., 2012, **18**, 66.
13 L.G. Chagas, D. Buchholz, L. Wu, B. Vortmann, S. Passerini, *J. Power Sources*, 2014, **247**, 377.
14 N. Yabuuchi, M. Kajiyama, J. Iwatate, H. Nishikawa, S. Hitomi, R. Okuyama, R. Usui, Y. Yamada, S. Komaba, *Nat. Mater*., 2012, **11**, 512.
15 D. Kim, S.-H. Kang, M. Slater, S. Rood, J.T. Vaughey, N. Karan, M. Balasubramanian, C.S Johnson, *Adv. Energy Mat*., 2011, **1**, 333.
16 S. Komaba, C. Takei, T. Nakayama, A. Ogata, N. Yabuuchi, *Electrochem. Commun*., 2010, **12**, 355.
17 M. Dollé, S. Patoux, M.M. Doeff, *Chem. Mater*., 2005, **17**, 1036.
18 J.M Paulsen, J.R. Dahn, *J. Electrochem. Soc*., 2000, **147** (7), 2478.
19 J.M Paulsen, J.R. Dahn, *Solid State Ionics*, 1999, **126**, 3.
20 J.M. Paulsen, R.A Donaberger, J.R. Dahn, *Chem. Mater*., 2000, **12**, 2257.
21 R. Berthelot, D. Carlier, C. Delmas, *Nat. Mater*., 2011, **10**, 74.

22 S. Komaba, N. Yabuuchi, T. Nakayama, A. Ogata, T. Ishikawa, I. Nakai, *Inorg. Chem*., 2012, **51**, 6211.
23 Z. Lu, J.R. Dahn, *J. Electrochem. Soc*., 2001, **148** (11), A1225.
24 Z. Lu, J.R. Dahn, *J. Electrochem. Soc*., 2001, **148** (7), A710.
25 Y.S. Meng, Y. Hinuma, G.J. Ceder, *Chem. Phys*., 2008, **128**, 104708-1.
26 P. Zhang, R.B. Capaz, M.L. Cohen, S.G. Louie, *Phys. Rev. B*, 2005, **71**, 153102-1.
27 Y. Wang, Y. Ding, J. Ni, *J. Phys.: Condens. Matter*, 2009, **21**, 035401-1.
28 H.W. Zandbergen, M. Foo, Q. Xu, V. Kumar, R.J. Cava, *Phys. Rev. B*, 2004, **70**, 024101-1.
29 M. Roger, D.J.P. Morris, D.A. Tennant, M.J. Gutmann, J.P. Goff, J.-U. Hoffmann, R. Feyerherm, E. Dudzik, D. Prabhakaran, A.T. Boothroyd, N. Shannon, B. Lake, P.P. Deen, *Nature Lett*., 2004, **8**, 631.
30 Z.Lu, J.R. Dahn, *Chem. Mater*., 2001, **13**, 1252.
31 A. Caballero, L. Hernán, J. Morales, L. Sánchez, J. Santos Peña, M.A.G. Aranda, *J. Mater. Chem*., 2002, **12**, 1142.
32 D. Lee, H. J.Xu, Y.S. Meng, *Phys.Chem. Chem. Phys*., 2013, **15**, 3304.
33 Z. Lu, R.A. Donaberger, J.R. Dahn, *Chem. Mater*., 2000, **12**, 3583.
34 J. Cabana, N.A. Chernova, J. Xiao, M. Roppolo, K.A. Aldi, M.S. Whittingham, C.P. Grey, *Inorg. Chem*., 2013, **52**, 8540.
35 Z. Lu, R.A. Donaberger, C.L. Thomas, J.R. Dahn, *J. Electrochem. Soc*., 2002, **149** (8), A1083.
36 H. Kaftelen, M. Tuncer, S. Tu, S. Repp, H. Göçmez, R. Thomann, S. Weber, E. Erdem, *J. Mater. Chem. A*, 2013, **1**, 9973-9982.